Surfaces and Interfaces 35 (2022) 102428

Contents lists available at ScienceDirect

Surfaces and Interfaces

journal homepage: www.sciencedirect.com/journal/surfaces-and-interfaces

Enhanced formation of nanometric titanium cones by incorporation of titanium, tungsten and/or iron in a helium ion beam

Fabien Sanchez [a,*], R. Steiner [a], P. Lattner [a], J. Spicher [a], D. Mathys [f], R. Antunes [a], M. Kisiel [a], K. Mukaddam [b], M. Astasov-Frauenhoffer [c], S. Kühl [b], J. Köser [d], R.S. Wagner [e], L. Marot [a], E. Meyer [a]

[a] Department of Physics, University of Basel, Klingelbergstrasse 82, CH-4056, Basel, Switzerland
[b] Department of Oral Surgery, University Center for Dental Medicine Basel (UZB), University of Basel, Mattenstrasse 40, 4058 Basel, Switzerland
[c] Department Research, University Center for Dental Medicine Basel (UZB), University of Basel, Mattenstrasse 40, 4058 Basel, Switzerland
[d] School of Life Sciences, Institute for Bioanalytics, University of Applied Sciences and Arts Northwestern Switzerland, Hofackerstrasse 36, 4132 Muttenz, Switzerland
[e] Institut Straumann AG, Basel, Switzerland
[f] Swiss Nanoscience Institute, University of Basel, Klingelbergstrasse 50/70, CH-4056, Basel, Switzerland

ARTICLE INFO

Keywords:
Nanometric cones
Helium ions
Unbalanced magnetron sputtering
High-flux ion source
Surface engineering

ABSTRACT

Surface patterning of bio-compatible titanium (Ti) shows a growing interest in the medical field. The engineering of material surfaces can achieve bactericidal properties and osteointegration improvements in order to develop medical implants. Spikes-like surface morphologies have already demonstrated the development of promising bactericidal properties. A barely new method to produce nanometric-sized cones on titanium consists of helium (He) ion irradiation using low energies (≈100 eV) and temperatures comprised between $0.25 < T/T_m < 0.5$ (with T_m being the melting temperature of the material). Ti, iron (Fe) and/or tungsten (W) were incorporated in a He beam, and their amounts were quantified using X-ray Photoelectron Spectroscopy (XPS). The He ion energy was varied from 70 and 120 eV, the surface temperatures from 571 to 651 K for fluences approximately equal to 10^{24} m^{-2}. After irradiation, the surface morphology was characterized using Scanning Electron Microscopy (SEM) and Focused Ion Beam (FIB). This study demonstrated the capability for irradiated Ti surfaces to form cones with tunable density, aspect ratio, and heights with the incorporation of Ti, Fe and/or W in a He ion. Additionally, the growth rate of the cones was enhanced by about 30 times in comparison to pure He irradiation as a function of the chosen materials introduced in the He beam.

1. Introduction

Bactericidal properties were observed on insects such as cicada [1] or gecko [2] due to their wings or skin nano-/micro-structures preventing bacterial colonization and growth. This effect is induced by the contact between the bacterial membrane and the microstructure that increases the stress applied to the bacteria membranes, thus leading to their deformation and/or rupture [3]. Developing implants with similar bactericidal properties using bio-materials is of great interest for the medical field. The nanopatterning of titanium (Ti) implants is a promising method to improve osteointegration while hindering bacterial growth and the formation of biofilms. Various nanoscale modifications were achieved on Ti surfaces and demonstrated bactericidal effects for a wide range of dimensions and morphologies [4,5], including nanoflowers [6], nanowires [7], nanotubes [8,9], nano-ripples [10] and nanopillars [11]. More recently, nanocones were formed on Ti surfaces and achieved bactericidal properties [12].

Mukaddam et al. [12] reported the formation of nanocones by low-energy (≈100 eV) helium (He) ion irradiation on Ti surfaces. During the irradiation process, He diffuses as single-atoms in the bulk material. Most likely, He atoms bound to vacancy leading to the formation of an immobile He-vacancy complex [13]. Afterwards, the He-vacancy complex grows by absorbing thermally mobile He clusters [14]. When the cluster accumulates enough He, Frenkel pairs (a self-interstitial and a vacancy) are generated and reduce the pressure inside the He bubble [15]. As more He bubbles grow in the material, dislocation loops are emitted from the bubble [16,17]. Voids are formed underneath the surface [18] and possibly lead to craters. Further irradiation

* Corresponding author.
E-mail address: fabien.sanchez@unibas.ch (F. Sanchez).

https://doi.org/10.1016/j.surfin.2022.102428
Received 8 July 2022; Received in revised form 3 October 2022; Accepted 20 October 2022
Available online 8 November 2022

induces the appearance of protrusions due to the bursting of the He bubbles on the surface. The surface morphology is changed to either pinholes, nanocones, microstructures or rough surfaces, as reported by Kajita et al. [19]. Interestingly, not all materials exhibit the formation of nanocones under He ion irradiation. Ti [19–22], beryllium [23], copper [24] and stainless steel [20,21] exhibited nanocones on their surfaces after irradiation, whereas tungsten (W) never exhibited cone structures formed on its surface [25–29]. It is suspected that the sputtering yield [30] and the shear modulus [31] of the materials may have a considerable influence on the evolution of the surface morphology, especially in cone development. Sputtering yields of about 10^{-2} (for ion energies below 100 eV) and shear modulus below ≈ 80 GPa (for temperatures around 0.3 of the ratio surface temperature T over titanium melting temperature T_m) favoured the formation of cones.

Kajita et al. [19] reported the formation of nanocones by irradiating Ti samples by means of He ion energies comprised between 69 and 90 eV, substrate temperatures between 520 and 1200 K and fluences above 1.5×10^{25} m^{-2}. Miyaguchi et al. [22] investigated the effects of Ti partially ionized (from 20 to 57%) deposited during 85 eV He ion bombardment. The surface temperature was ≈ 850 K and the He fluence ≈ 6.0×10^{25} m^{-2}. The ionization degree and the amount of Ti deposited played a significant role in the final topology.

The incident He ion energy, substrate temperature, fluence and the incorporated materials during the irradiation lead to surface morphology changes through the cone density, heights and/or their aspect ratios. There is growing evidence that the previously mentioned surface characteristics play an important role in the bactericidal properties of the material. In our contribution, nanocones were formed on the Ti substrate while Ti, iron (Fe) and W were incorporated in a He beam. Additionally, the effect of the He ion energy and the substrate temperature in the case of W/Fe incorporated in a He beam was investigated. This work demonstrates the capability to tune the nanocones' characteristics in terms of density, aspect ratios and heights. Moreover, nanocones were successfully formed using fluences one order of magnitude lower than pure He irradiation. Finally, the mechanisms leading to nanometer-scale changes and the growth rate enhancement compared to pure He irradiation will be discussed.

2. Material and methods

Titanium discs of 15 mm diameter having a machined surface with an arithmetical roughness (R_a) of 140 nm were placed in a high vacuum chamber with a base pressure better than 10^{-5} Pa and exposed to He ions irradiation. Two different sources were used to produce the He ions:

- unbalanced magnetron sputtering (UBM) consisting of opening the magnetic field lines of a traditional magnetron sputtering system. In our case, the unbalancing of the magnetic field lines were induced by the addition of electromagnetic coils surrounding the UBM system. The He ions were generated at the magnetron target, extracted from the target region and guided onto the samples leading to He fluxes of around 10^{19} m^{-2} s^{-1}. Simultaneously, the magnetron target was eroded and material was introduced in the He beam.
- ion source (KRI EH-1000, manufactured by Kaufman & Robinson, Inc., USA) in which a discharge current is applied to the anode (Fig. 1) in an optimized configuration in order to produce He fluxes of around 10^{20} m^{-2} s^{-1}.

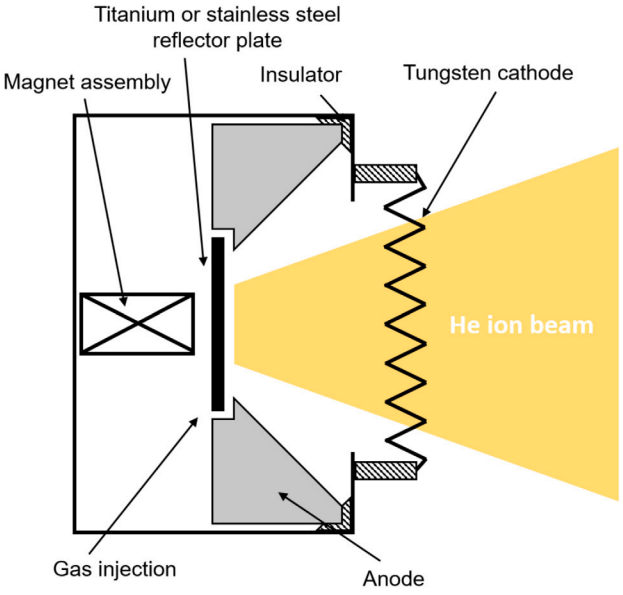

Fig. 1. Schematic of the eH1000 ion source.

Those methods make possible to add various materials (being either ions or neutrals) in the He beam and vary their amounts in order to observe the morphology changes on Ti substrates. Additionally, the eH1000 ion source was used to generate higher He fluxes compared to UBM (by a factor of 5). The UBM and the ion source working conditions are described in more detail in their dedicated sections.

Due to the He irradiation, heat flux is generated and delivered to the samples. The samples' surface temperature was monitored using a thermocouple directly contacted onto the sample holder. This last was cooled or heated depending on the targeted temperature and the He ion flux. Moreover, the stage was biased in order to adjust the energy of the incident He ions. A retarding field energy analyser (RFEA, model Semion Single Sensor, Impedans) was used to quantify the He ion fluxes and the ion energies. After irradiation, the titanium sample surface morphology was investigated using Scanning Electron Microscopy (SEM, Hitachi S4-800) and Focused Ion Beam (FIB, Helios NanoLab 650).

2.1. Unbalanced magnetron sputtering

The UBM system is a magnetron sputtering system with additional solenoid coils in its surroundings to unbalance the inner and outer magnets, leading to an opening of the magnetic field lines as described in [32]. Consequently, the He plasma was not confined around the target, but rather guided onto the samples in a beam fashion [33,34]. A titanium target of 23 mm diameter was used, and the plasma was

Table 1
The structuring method, the material provided in the He beam and irradiation conditions of the Ti discs used in this work. The ratio $\frac{T}{T_m}$ was calculated using the melting temperature (T_m) equal to 1941 K.

Samples	Structuring method	Elements	Temperature (K)	Ratio T/T_m	Ion energy (eV)	Flux (10^{19} $m^{-2}s^{-1}$)	Time (h)	Fluence (10^{24} m^{-2})
Ti-1	UBM	Ti	620	0.32	120	2.08	24	1.80
Ti-2	eH1000	W	605	0.31	100	5.60	24	4.84
Ti-3	eH1000	W/Fe	612	0.32	70	10.30	5.5	2.04
Ti-4	eH1000	W/Fe	614	0.32	100	10.30	5.5	2.04
Ti-5	eH1000	W/Fe	611	0.31	120	10.30	5.5	2.04
Ti-6	eH1000	W/Fe	571	0.29	100	10.30	5.5	2.04
Ti-7	eH1000	W/Fe	651	0.34	100	10.30	5.5	2.04

excited with a 50 W power delivered by a DC generator operated in pulsed mode. The pulse width and frequency were equal to 496 ns and 5 kHz, respectively. The pressure was equal to 0.85 Pa, resulting in a He ion flux of 2.08 × 10^{19} m^{-2} s^{-1} measured by the RFEA. The Ti target is sputtered, leading to a deposition rate of 1.7 pm s^{-1} as measured by a Quartz Microbalance (QMB).

2.2. Ion source

The He ions produced by the eH1000 ion source were generated by a discharge voltage of V_d = 115 V and a discharge current of I_d = 3 A delivered to the anode. The He flux generated ranged between 5.60 × 10^{19} $m^{-2}s^{-1}$ and 1.03 × 10^{20} $m^{-2}s^{-1}$ which is at least 3 times higher than the He flux provided by the UBM. A schematic of the eH1000 is provided in Fig. 1. In the eH1000 ion source, the He gas is injected through the reflector side and gets ionized at the anode. The majority of the ions flow outside of the source, contributing to the ion beam. However, some ions are directed backwards against the reflector plate [35]. Consequently, the reflector material can be sputtered in the He beam. In our study, the reflector plate was made of Ti for Ti-2 and stainless steel for Ti-3 to Ti-7 (Table 1). The latter leads to the addition of Fe in the beam.

In addition, a cathode was installed in a sidewinder configuration in front of the ion source (Fig. 1) and provided electrons to neutralize the space charge of the ions. The cathode is a 99.95% pure W wire with a section of 0.5 mm in which a current of about 20 A is loaded. The pressures during irradiation were in the range of 0.53 and 0.58 Pa. Under these conditions, the W wire is heated and thus evaporated in the He beam.

X-ray Photoelectron Spectroscopy (XPS, VG ESCALAB 210 spectrophotometer using monochromatized Al kα, hν = 1486.6 eV) analysis were systematically performed of the irradiated Ti samples in order to quantify the amount of W or W/Fe on the Ti substrates after He irradiation. It is worth noticing that the other elements present in stainless steel (i.e., nickel, chromium) remained below detection limit of the XPS.

3. Results

3.1. Post-irradiation surface composition

The amount of material deposited using the eH1000 ion source was quantified using XPS. Its total was found to be dependent on the source parameters (i.e. discharge voltage, discharge current, filament current and working pressure) and the He irradiation time. Ti-3 to Ti-7 were subject to the same irradiation times and source parameters to achieve a similar amount of W and Fe on their surfaces, as reported in Table 2. Similar quantification was performed on Ti-2 exhibiting 16 at. % of W. For the UBM, the Ti deposition rate was measured by the aims of QMB and was equal to 1.7 pm s^{-1}.

Table 2
Surface composition of the W and the W/Fe irradiated discs using the ion source. The titanium amounts corresponds to the contribution of the substrate. Wide scan XPS spectra also showed carbon and oxygen and were not considered for the surface composition since their amounts correspond to air contamination.

Samples	Surface composition (at. %)		
	W	Fe	Ti
Ti-2	16	0	84
Ti-3 to Ti-7	4	46	50

3.2. Elements incorporated in a He ion beam

Fig. 2 shows SEM images of the Ti surfaces Ti-1, Ti-2 and Ti-4 after He ion irradiation. The temperature used in this study was around 610 K, which corresponds to around 0.31 of the ratio $\frac{T}{T_m}$. The He ion energies were equal to 100 eV for Ti-2 and Ti-4 whereas Ti-1 was subject to 120 eV ion energy. In this study, Ti, W or W/Fe were incorporated in a He beam. W was chosen because of its high sputtering energy threshold (above the 120 eV He ion energy used in this study). Fe was sputtered in addition to W because of its capability to develop cones by pure He ion irradiation and its similar physical properties compared to Ti (Table 3). After irradiation, the surface morphologies were analysed in terms of cone density, aspect ratio, heights and growth rate.

The cone density was determined after statistical analysis using Image J software on the SEM images (Fig. 2). In the case of Ti in

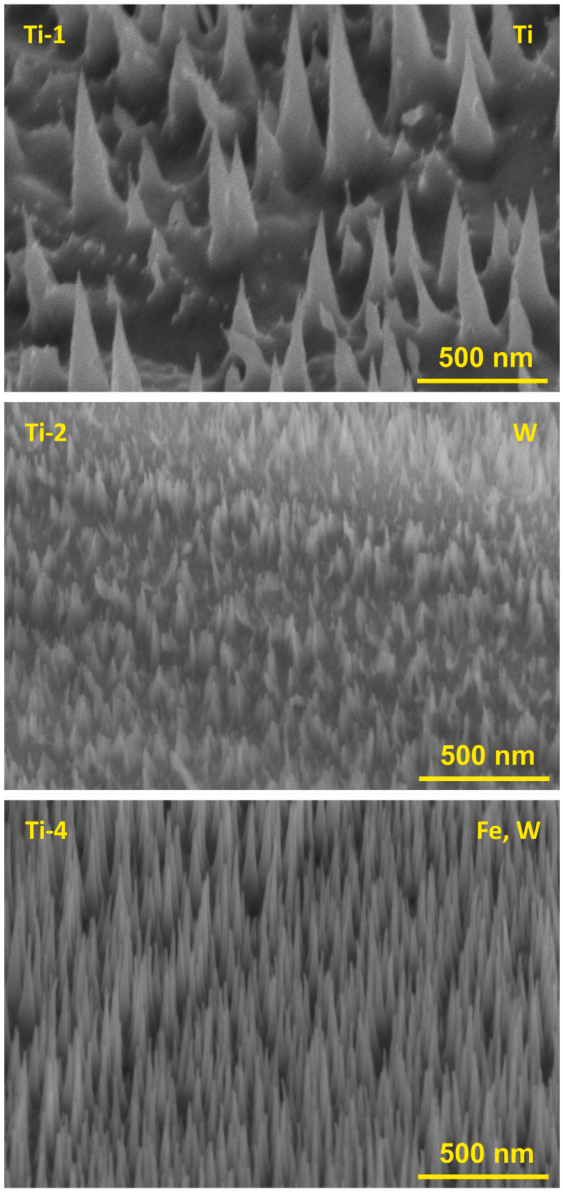

Fig. 2. Tilted views (52°) SEM images of Ti-1, Ti-2 and Ti-4. Samples were irradiated by aims of He fluences comprised between 1.80 × 10^{24} m^{-2} and 4.84 × 10^{24} m^{-2}. Simultaneous incorporation of Ti, W and W/Fe were performed during the He ion bombardment on Ti-1, Ti-2 and Ti-4, respectively.

Table 3
Physical properties of Ti, Fe and W. The shear modulus values corresponds to the material bulk characteristics at room temperature and without incorporation of He.

Material	Melting temperature (K)	Shear Modulus (GPa)	Sputter yield 70 eV	100 eV	120 eV	Sputter energy threshold (eV)
Titanium	1941	41–44	0.007	0.013	0.018	25
Iron	1811	82	0.015	0.030	0.039	24
Tungsten	3695	161	0	0	0	155

the He beam, the cone density was 25 cones per μm^2 which is in the range of 10 to 70 cones per μm^2 reported by Kajita et al. for pure He irradiation [19]. The addition of W and W/Fe increased the cones' density to 180 and 270 cones per μm^2, respectively.

Average peak heights of 450, 140 and 340 nm were determined for Ti-1, Ti-2 and Ti-4 after statistical analysis of the SEM images (Fig. 2). Since the samples were subject to various fluences (Table 1), the heights of the cones cannot be directly compared. Therefore, a growth rate was calculated using the cone heights divided by their respective He fluences. The resulting growth yields for Ti, W and W/Fe were equal to 2.5, 0.29 and 1.7×10^{-31} m^3, respectively. In comparison, Kajita et al. [19] reported the formation of nanocones of around 139 nm height using He ions energy of 90 eV, surface temperature of 600 K and fluence of 15 $\times 10^{24}$ m^{-2} leading to a growth rate of around 0.09 $\times 10^{-31}$ m^3. In our work, adding Ti and W/Fe in a He ion beam increased the growth rate by a factor of 28 and 19 compared to a pure He irradiation [19]. For the W case, the growth rate remained close to pure He irradiation, albeit the growth rate was improved by a factor of 3.

The base width of the cones was measured using SEM images (Fig. 2), allowing to calculate the aspect ratio of the cones by dividing their heights by their base widths. The cone's aspect ratio changes depending on the material inserted in the He beam. Aspect ratios of 2.8, 3.9 and 6 were calculated for the Ti, the W and the W/Fe cases, respectively. The mechanisms leading to the cone morphology differences will be assessed in the discussion part.

3.3. Nanocone formation: influence of the he ion energy during irradiation with W/Fe incorporated in a He beam

In Fig. 3, Ti surfaces were irradiated by He ions in which Fe and W were incorporated. For this study, the fluence was kept constant and equal to 2.04×10^{24} m^{-2}. The samples surface's temperatures were fixed at around 610 K (≈ 0.31 $\frac{T}{T_m}$). The specimens were irradiated by He ions having energies comprised between 70 and 120 eV and cones were observed in the entire He energy range. For ion energies from 70 to 100 eV, the cone heights increased from 175 to 340 nm. At 120 eV, the surface exhibited the coexistence of peaks having 370 and 200 nm leading to an average of 310 nm. The coexistence of two cone sizes was not observed for the He ion energy of 70 and 100 eV. The cones' aspect ratios of 6 and their density (≈ 250 cones per μm^2) were not affected by the change in ion energy.

3.4. Nanocone formation: influence of the substrate surface temperature during irradiation with W/Fe incorporated in a He beam

Similarly to the previous section, W/Fe were incorporated in a He ion beam and irradiated Ti samples. The fluence and the ion energy were kept constant and equal to 2.04×10^{24} m^{-2} and 100 eV. The surface temperature of the samples were varied from 571 to 651 K and corresponded to around 0.29 and 0.34 of the ratio $\frac{T}{T_m}$. In Fig. 4, nanocones were formed in the whole range of studied temperature. The temperature did not influence the aspect ratio and density of the cones, whereas their heights were equal to 260, 340 and 310 nm for surface temperatures of 571, 614 and 651 K, respectively.

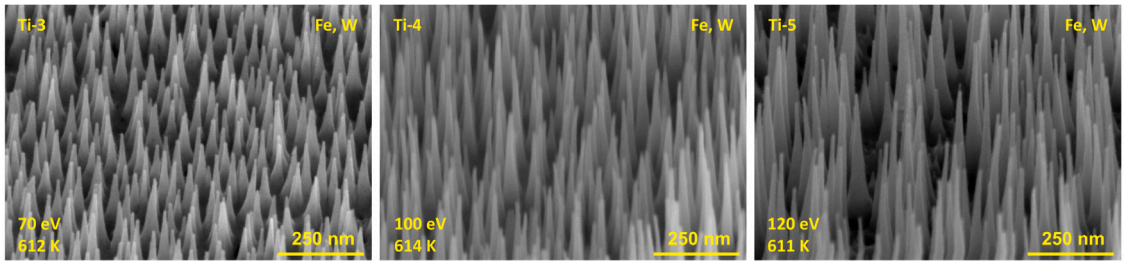

Fig. 3. Tilted views (52°) SEM images of Ti-3, Ti-4 and Ti-5. The Ti specimens were irradiated by He ions having energies of 70, 100 and 120 eV for Ti-3, Ti-4 and Ti-5, respectively. The He fluences and specimens' temperatures were kept constant and equal to 2.04 $\times 10^{24}$ m^{-2} and around 610 K. Fe and W were incorporated in the He beam during the irradiation.

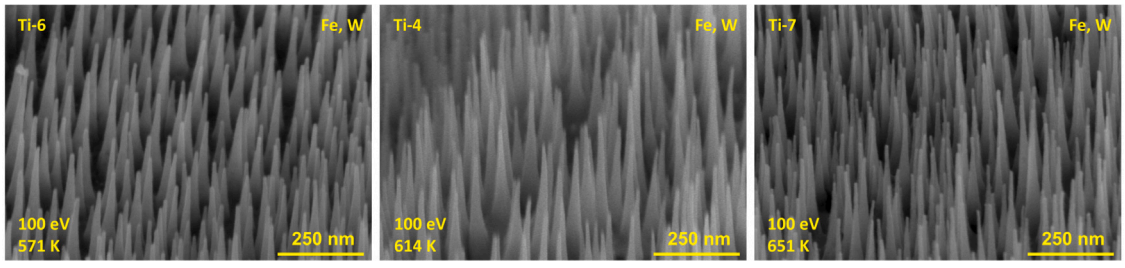

Fig. 4. Tilted views (52°) SEM images of Ti-6, Ti-4 and Ti-7. The Ti specimens were irradiated by He ions having energies of 100 eV and fluences equal to 2.04 $\times 10^{24}$ m^{-2}. The temperatures of the Ti discs were equal to 571, 614 and 651 K for Ti-6, Ti-4 and Ti-7, respectively. Fe and W were incorporated in the He beam during the irradiation.

4. Discussion

4.1. Surface effects on titanium

As previously explained, the He atoms are implanted in the material, creating He blisters. FIB was carried out and displayed in Fig. 5 to visualize the He bubbles. Most of the He bubbles were observed in the cones with diameters between 15 and 80 nm. Smaller diameter bubbles were not observed due to the redeposition of the sputtered material during the FIB process. He bubbles were found with diameters around 150 nm in the cones. He bubbles thermally migrate, leading to protrusions via bursting on the surface [31,36,37]. When protrusions are formed on the surface, the He ions no longer irradiate the surface normally ($\theta = 0°$) but with an angle θ. By simple geometric consideration, θ is also the angle between the initial flat surface and the cone slope (Fig. 5). At that state, Bradley–Harper instability [38], the angular dependence of sputtering yield [39] and the surface stress induced by the ions drive the nanocones' growth [40].

Begrambekov et al. [40] reported the influence of a critical angle θ_c in respect to θ on the cone morphology. When θ_c is higher than θ, surface stress appears on the cone slope and creates an atom diffusion flow to the top of the cone. It is worth mentioning that the He diffusion and coalescence require surface temperature comprised between $0.25 < \frac{T}{T_m} < 0.5$. In these conditions, surface diffusion is activated. Begrambekov et al. [40] reported a relation between θ and E_m which is the energy to produce interstitial in the near-surface region:

$$E_m = E_i \frac{4M_1M_2}{(M_1+M_2)^2} cos^2(\theta_{cr}) \quad (1)$$

Where E_i is the incident ion energy, M_1 is the mass of a He atom and M_2 is the mass of the encountered atom (Ti for the pure He ion irradiation). In the case of Ti in the He beam, E_i was equal to 120 eV and the energy E_m to form a complex He-vacancy in Ti material is comprised between 2.5 and 3 eV depending on the trapping site and the potentials used for the calculation [14,41]. Using the previous parameters, θ_{cr} is about 73°. With the value of θ_{cr}, we obtained an aspect ratio of around 3.4. Experimentally, we estimated a value of 2.8 ± 0.12, which is close to the calculated one. Moreover, the aspect ratio only depends on the material and the ion energy. Consequently, the aspect ratio is conserved while sweeping the surface temperature, as observed in Fig. 4. The aspect ratio is expected to change as a function of the ion energy. Using Eq. (1) with 70 eV, the calculated aspect ratio decreases to around 2.5 instead of 3.4 for 120 eV He ion energy. In our study, no change in the aspect ratio was observed between 70 and 120 eV ion energies. It is worth noticing that our experimental value lies within the calculated range showing the possibility of predicting the cones' aspect ratio.

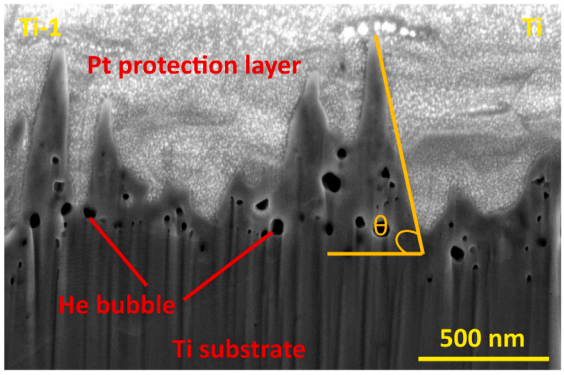

Fig. 5. FIB cross-section of Ti-1 irradiated by He ions. Cones exhibited nanometric He bubbles after irradiation. A platinum (Pt) layer was deposited prior to the FIB cross-section in order to protect the material surface.

In the case of Ti in a He beam, the growth yields were 10 times higher than pure He irradiation. The increase of the growth yield can be explained by the protrusions formed at an earlier stage and the addition of materials that are free from stress and give the material the capability to accumulate more He.

4.2. W introduction in the He beam

When W or W/Fe are introduced in a He beam, E_m and the surface atoms may differ (depending on the encountered atoms and probably on the amounts of the incorporated materials), leading to aspect ratio variations. Moreover, as the W sputter energy threshold using He gas is 155 eV and the He ion energy is only 120 eV, W is not sputtered from the surface (Table 3). In the early stages, W was deposited on the surface, leading to protrusions. Similarly to the previous section, surface diffusion and Ti sputtering led to cone formation on the surface. However, in the present case, W induced protrusions which cannot be sputtered away. Consequently, W was the starting point for cone formation and is expected to be located on their summits, as reported by Shi et al. [42]. The cone density is directly linked to the initial number of protrusions formed on the surface. Thereby, the cone density and the aspect ratio increased from 10–70 to 200 cones per μm^2 and from 2.8 to 6 compared to pure He ion bombardment [19], respectively. Finally, the cone growth yields of cones using W in a He beam or pure He irradiation were similar, albeit the protrusions were formed earlier for the W case. The W impedes the incorporation and the desorption of He and leads to nanocones having similar growth yields compared to pure He irradiation.

As reported in Table 3, Fe has similar properties to those of Ti (i.e., melting point and sputter yield), making surface and He diffusion activated at temperatures around 600 K and ion energies below 120 eV [43]. Moreover, Fe already showed its capability to develop cones on its surface by He irradiation [21]. Adding Fe in a He beam with W combines lower cone densities obtained with W, while the growth yields remained in the same order of magnitude compared to Ti in a He beam.

4.3. Nanocone surface engineering

In Fig. 6, the cones' growth yields are plotted for different materials incorporated in the He beam, surface temperatures and ion energies.

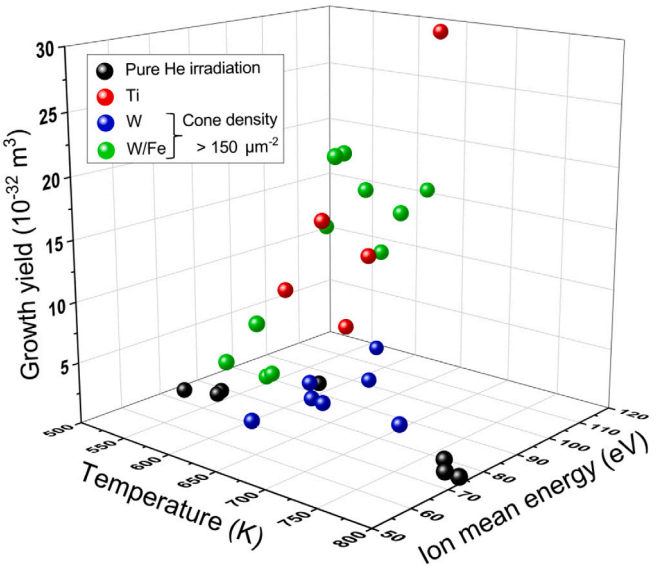

Fig. 6. Nanocones growth yield (cone height divided by ion fluence) plotted as function of temperature and ion energy for pure He bombardment [19] and with Ti, W and W/Fe in the He beam.

The results obtained by Kajita et al. [19] in the case of a pure He irradiation were added. As mentioned previously, the growth yields increased while adding Fe or Ti in the He beam and remained one order of magnitude lower when only W was added. The latter exhibited similar growth yields in comparison to pure He irradiation. When Fe was added to W, a similar growth yield was measured compared to Ti in a He beam. The addition of material in the beam can be used to tune the cones' growth yields, aspect ratio and density. This study highlights the influence of the surface diffusion and sputtering process on the morphology of the cone and, therefore, the material's sputtering yield and melting point. Moreover, the growth yields of the cones can be tuned by the sample temperature and He ion energy however it did not influence the cones' density and aspect ratio.

5. Conclusions

Nanocones were successfully structured on Ti surfaces after exposure to He ion bombardment in the presence of Ti, Fe or W in a He beam. This work exhibits the capability to tune the cone characteristics by modifying the substrate temperature, the He ion energy and/or by adding materials to the He beam. Ti, W and W/Fe were incorporated in a He beam and drastically affected the surface morphology through the cones' density, heights, aspect ratios and growth yields. The addition of Ti in the He beam led to similar cone density compared to pure He irradiation [19] whereas the cones' growth yields increased by a factor of 30. Now considering the addition of W, the growth rate was similar to pure He irradiation, whereas the cone density increases from around 50 to 200 cones per μm^2. The addition of Fe in addition to W in a He beam increased the cone's growth yields by a factor of 15 while conserving the cone density compared to W in a He beam. The previously mentioned differences in the cones' characteristics can be explained by the physical properties of the materials and especially their sputtering yields. The W sputtering energy threshold being higher than the ion energies used in this study, the W cannot be sputtered from the surface. Thus, protrusions produced by the W deposited on the surface remained on the surface and favoured the formation of dense structures. Moreover, when adding Ti in a pure He beam or incorporating Fe in a He ion beam containing W, the addition of elements with a sputtering energy threshold lower than the He ion energy enhanced the formation of the cones.

Moreover, He ion energy variation from 70 to 120 eV and temperature in the range of 570 to 650 K modified the cones' growth yields by a factor less than 2. In contrast, the cones' density and aspect ratios were not affected.

CRediT authorship contribution statement

Fabien Sanchez: Writing – original draft, Investigation, Formal analysis, Visualization. **R. Steiner:** Investigation, Methodology. **P. Lattner:** Investigation, Visualization. **J. Spicher:** Investigation, Visualization. **D. Mathys:** Investigation. **R. Antunes:** Supervision, Writing – review & editing. **M. Kisiel:** Investigation, Conceptualization. **K. Mukaddam:** Conceptualization. **M. Astasov-Frauenhoffer:** Conceptualization. **J. Köser:** Conceptualization. **R.S. Wagner:** Conceptualization, Resources. **L. Marot:** Supervision, Project administration, Funding acquisition, Formal analysis, Writing – review & editing. **E. Meyer:** Project administration, Funding acquisition.

Declaration of competing interest

One or more of the authors of this paper have disclosed potential or pertinent conflicts of interest, which may include receipt of payment, either direct or indirect, institutional support, or association with an entity in the biomedical field which may be perceived to have potential conflict of interest with this work. For full disclosure statements refer to https://doi.org/10.1016/j.surfin.2022.102428. Laurent Marot reports financial support was provided by University of Basel Swiss Nanoscience Institute. Ernst Meyer reports financial support was provided by Swiss National Science Foundation. Ernst Meyer reports financial support was provided by European Research Council.

Data availability

Data will be made available on request.

Acknowledgements

This work was supported by the Swiss Nanoscience Institute through the nano-Argovia project "TiSpikes A15.11". We also thank the Swiss National Science Foundation (SNF) and the European Research Council (ERC) under the European Union's Horizon 2020 research and innovation program (ULTRADISS grant agreement No. 834402).

References

[1] E.P. Ivanova, J. Hasan, H.K. Webb, V.K. Truong, G.S. Watson, J.A. Watson, V.A. Baulin, S. Pogodin, J.Y. Wang, M.J. Tobin, et al., Small 8 (16) (2012) 2489–2494.
[2] G.S. Watson, D.W. Green, L. Schwarzkopf, X. Li, B.W. Cribb, S. Myhra, J.A. Watson, Acta Biomater. 21 (2015) 109–122.
[3] S. Pogodin, J. Hasan, V.A. Baulin, H.K. Webb, V.K. Truong, T.H.P. Nguyen, V. Boshkovikj, C.J. Fluke, G.S. Watson, J.A. Watson, et al., Biophys. J. 104 (4) (2013) 835–840.
[4] J. Liu, J. Liu, S. Attarilar, C. Wang, M. Tamaddon, C. Yang, K. Xie, J. Yao, L. Wang, C. Liu, et al., Front. Bioeng. Biotechnol. (2020) 1314.
[5] K. Modaresifar, S. Azizian, M. Ganjian, L.E. Fratila-Apachitei, A.A. Zadpoor, Acta Biomater. 83 (2019) 29–36.
[6] J. Vishnu, V.K. Manivasagam, V. Gopal, C.B. Garcia, P. Hameed, G. Manivasagam, T.J. Webster, Nanomedicine: Nanotechnol. Biol. Med. 20 (2019) 102016.
[7] A. Jaggessar, A. Mathew, H. Wang, T. Tesfamichael, C. Yan, P.K. Yarlagadda, J. Mech. Behav. Biomed. Mater. 80 (2018) 311–319.
[8] S. Rahnamaee, R. Bagheri, M. Vossoughi, S.A. Seyedkhani, A. Samadikuchaksaraei, Ceram. Int. 46 (7) (2020) 9669–9679.
[9] V. Simi, N. Rajendran, Mater. Charact. 129 (2017) 67–79.
[10] X. Luo, S. Yao, H. Zhang, M. Cai, W. Liu, R. Pan, C. Chen, X. Wang, L. Wang, M. Zhong, Opt. Laser Technol. 124 (2020) 105973.
[11] D.P. Linklater, S. Juodkazis, R.J. Crawford, E.P. Ivanova, Materialia 5 (2019) 100197.
[12] K. Mukaddam, M. Astasov-Frauenhoffer, E. Fasler-Kan, L. Marot, M. Kisiel, R. Steiner, F. Sanchez, E. Meyer, J. Köser, M.M. Bornstein, et al., Nanomaterials 12 (7) (2022) 1065.
[13] Y.-l. Wang, S. Liu, L.-j. Rong, Y.-m. Wang, J. Nucl. Mater. 402 (1) (2010) 55–59.
[14] A.Y. Kuksin, A. Rokhmanenkov, V. Stegailov, Phys. Solid State 55 (2) (2013) 367–372.
[15] M. Abd El Keriem, D. Van Der Werf, F. Pleiter, Hyperfine Interact. 79 (1) (1993) 787–791.
[16] F. Sefta, K.D. Hammond, N. Juslin, B.D. Wirth, Nucl. Fusion 53 (7) (2013) 073015.
[17] L. Sandoval, D. Perez, B.P. Uberuaga, A.F. Voter, Fusion Sci. Technol. 71 (1) (2017) 1–6.
[18] S. Iyyakkunnel, L. Marot, B. Eren, R. Steiner, L. Moser, D. Mathys, M. Duggelin, P. Chapon, E. Meyer, ACS Appl. Mater. Interfaces 6 (14) (2014) 11609–11616.
[19] S. Kajita, D. Kitaoka, N. Ohno, R. Yoshihara, N. Yoshida, T. Yoshida, Appl. surf. sci. 303 (2014) 438–445.
[20] S. Kajita, T. Saeki, Y. Hirahata, N. Ohno, Japan. J. Appl. Phys. 50 (1S1) (2011) 01AH02.
[21] S. Kajita, T. Yoshida, D. Kitaoka, R. Etoh, M. Yajima, N. Ohno, H. Yoshida, N. Yoshida, Y. Terao, J. Appl. Phys. 113 (13) (2013) 134301.
[22] K. Miyaguchi, S. Kajita, H. Tanaka, N. Ohno, Japan. J. Appl. Phys. 60 (3) (2021) 038004.
[23] R. Doerner, M. Baldwin, D. Nishijima, J. Nucl. Mater. 455 (1–3) (2014) 1–4.
[24] P. Fiflis, N. Connolly, D. Ruzic, J. Nucl. Mater. 482 (2016) 201–209.
[25] G. De Temmerman, K. Bystrov, J.J. Zielinski, M. Balden, G. Matern, C. Arnas, L. Marot, J. Vac. Sci. Technol. A: Vac. Surf. Films 30 (4) (2012) 041306.
[26] D. Dasgupta, R.D. Kolasinski, R.W. Friddle, L. Du, D. Maroudas, B.D. Wirth, Nucl. Fusion 59 (8) (2019) 086057.
[27] D. Hwangbo, S. Kajita, H. Tanaka, N. Ohno, Nucl. Mater. Energy 18 (2019) 250–257.
[28] S. Kajita, W. Sakaguchi, N. Ohno, N. Yoshida, T. Saeki, Nucl. Fusion 49 (9) (2009) 095005.
[29] L. Marot, J. Fleury, D. Haas, S. Iyyakkunnel, F. Sanchez, R. Steiner, D. Mathys, R. Antunes, E. Meyer, Surf. Coat. Technol. (2022) 128870.

[30] S. Kajita, T. Ishida, N. Ohno, D. Hwangbo, T. Yoshida, Sci. Rep. 6 (1) (2016) 1–10.
[31] S. Takamura, Y. Uesugi, Appl. surf. sci. 356 (2015) 888–897.
[32] T. Petty, A. Khan, T. Heil, J. Bradley, J. Nucl. Mater. 480 (2016) 374–385.
[33] I. Svadkovski, D. Golosov, S. Zavatskiy, Vacuum 68 (4) (2002) 283–290.
[34] I. Ivanov, P. Kazansky, L. Hultman, I. Petrov, J.-E. Sundgren, J. Vac. Sci. Technol. A: Vac. Surf. Films 12 (2) (1994) 314–320.
[35] V.V. Zhurin, Industrial Ion Sources: Broadbeam Gridless Ion Source Technology, John Wiley & Sons, 2012.
[36] F. Sefta, N. Juslin, B.D. Wirth, J. Appl. Phys. 114 (24) (2013) 243518.
[37] P. Zhang, T. Zou, J. Zhao, J. Nucl. Mater. 467 (2015) 465–471.
[38] R.M. Bradley, J.M. Harper, J. Vac. Sci. Technol. A: Vac. Surf. Films 6 (4) (1988) 2390–2395.
[39] O. Auciello, J. Vac. Sci. Technol. 19 (4) (1981) 841–867.
[40] L. Begrambekov, A. Zakharov, V. Telkovsky, Nucl. Instrum. Methods Phys. Res. B 115 (1–4) (1996) 456–460.
[41] Y.-Y. Dai, L. Yang, S.-M. Peng, X.-G. Long, F. Gao, X.-T. Zu, Chin. Phys. Lett. 27 (12) (2010) 123102.
[42] Q. Shi, S. Kajita, S. Feng, N. Ohno, J. Phys. D: Appl. Phys. 54 (40) (2021) 405202.
[43] I. Tanyeli, L. Marot, M.C. van de Sanden, G. De Temmerman, ACS Appl. Mater. Interfaces 6 (5) (2014) 3462–3468.